

Paper

# Bifurcations in a forced Wilson–Cowan neuron pair

Masaki Yoshikawa <sup>1</sup>, Kentaro Ono <sup>1</sup>, and Tetsushi Ueta <sup>1</sup>

<sup>1</sup> Tokushima University, 2-1, Minami-Josanjima, Tokushima 770-8506, Japan

Received October 13, 2022; Revised December 28, 2022; Published April 1, 2023

**Abstract:** We investigate bifurcations of periodic solutions observed in the forced Wilson–Cowan neuron pair by both the brute-force computation and the shooting method. By superimposing the results given by both methods, a detailed topological classification of periodic solutions is achieved that includes tori and chaos attractors in the parameter space is achieved. We thoroughly explore the parameter space composed of threshold values, amplitude, and angular velocity of an external forcing term. Many bifurcation curves that are invisible when using brute-force method are solved by the shooting method. We find out a typical bifurcation structure including Arnold tongue in the angular velocity and the amplitude of the external force parameter plane, and confirm its fractal structure. In addition, the emergence of periodic bursting responses depending on these patterns is explained.

**Key Words:** Wilson–Cowan model, bifurcation, brute-force analysis, torus, chaos, entrainment

## 1. Introduction

Oscillations are a fundamental behavior in neuronal systems [1]. Many nonlinear phenomena related to oscillatory activities such as excitability changes, synchronizations, phase-locking phenomena, and bursting are observed from biological data in the brain. To explain these nonlinear oscillations theoretically and qualitatively, many mathematical models have been proposed and studied intensively for four decades. Various mathematical models have also been proposed to explain the above nonlinear oscillations. Hoppenstead and Izhikevich [2] classified canonical models describing such various oscillation modes with the bifurcation theory [1].

Among these oscillations, we are interested in nonlinear phenomena including resonance, bursting, or tori (quasi-periodic solutions) in forced inhibitory-excitatory neuron pair models from the perspective of bifurcation theory. In particular, we paid significant attentions to bifurcations of bursting responses in forced neuronal systems since they can be analyzed precisely by applying the Poincaré mapping. We investigated non-autonomous FitzHugh–Nagumo [3] and Amari–Hopfield [4] neuron models. Meanwhile, Wilson–Cowan (WC) neuron pairs [5] can also describe the dynamic behavior of spatially localized populations by combining excitatory and inhibitory neurons. Tsodyks et al. [6], Ermentrout and Terman [7], and Noonburg et al. [8] treat a periodically forced WC neuron pair motivated by [9]. Although the whole system can be written as a two-dimensional ordinary differential equation (ODE), by assuming a large amplitude oscillation and a low-frequency periodic force, it is



reduced into a single first-order ODE.

In [8], a periodical force is applied to the inhibitory neuron since paradoxical behavior in the rat hippocampus where the inhibitory cells receive external periodic inputs from analytical investigations, a rough bifurcation diagram (threshold space) is shown and a topological classification of periodic solutions are given; however, only the typical behavior of periodic solutions are classified since the reduction supposes very restricted oscillation conditions. Decker et al. [10] also shows the existence of multiple periodic attractors analytically and suggests that periodic forces applied to an excitatory neuron can change the topological properties of periodic solutions. Ledoux et al. [11] shows that nonlinear resonance occurs when either inhibitory-inhibitory pair or excitatory-inhibitory pair are near the Hopf bifurcation parameter. Very independent from the above neuronal studies, we also utilize this WC neuron model as a nonlinear oscillation unit to check the validity of numerical computation [12, 13] or control problem [14] examples.

Recently, Pérez-Cervera et al. [15] investigate phase-locked states (frequency entrainment regions) in a forced WC neuron pair as a mathematical model based on the communication through coherence theory. A phenomenological explanation of the population activity in the mean firing rate gives a mechanism underlying phase-locking in a neuronal cycle with different excitability phases. The results show that phase-locking states depending on the communication through coherence theory are confirmed, and the presence of bistable regions presents various communication regimes between brain areas. Some bifurcation diagrams in the frequency-amplitude of the external force are given.

From the above background, a thorough bifurcation analysis on the forced WC neuron pair can be expected. In this paper, we directly treat the non-autonomous differential equation describing the WC pair without any analytical assumptions and approximations and try to obtain bifurcation sets in various combinations of parameters with accurate numerical computations. Concretely, we investigate the topological properties qualitatively in threshold values, and the amplitude, the angular velocity of the forcing term. We feature two different computational tools to visualize bifurcation sets, namely the brute-force and the shooting methods. Superimposing results from these two methods visually clarifies bifurcation structures for any parameter plane.

## 2. Mathematical model

Figure 1 shows a schematic configuration of the WC neuron pair. The pair is interconnected by two cells, where  $E$  and  $I$  are the excitatory and inhibitory cells, respectively. The weights of synaptic connections are given by  $a$ ,  $b$ ,  $c$ , and  $d$  and the threshold values of excitable and inhibitory cells are  $\rho_x$  and  $\rho_y$ , respectively [16].

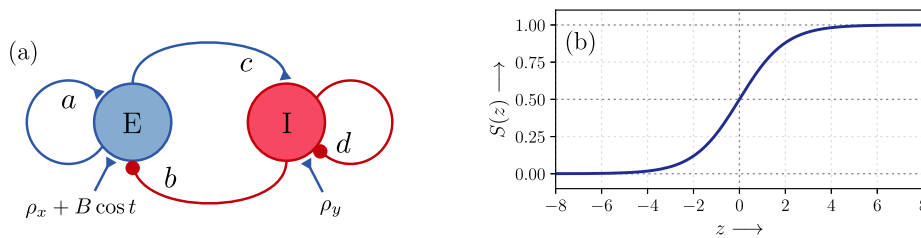


**Fig. 1.** Wilson–Cowan neuron pair. (a): schematic configuration, (b): the synaptic characteristics.

The WC neuron pair is described by the following ODE:

$$\begin{cases} \frac{dx}{dt} = -x + S(ax - by + \rho_x + B \cos \omega t) \\ \frac{dy}{dt} = -y + S(cx - dy + \rho_y), \end{cases} \quad (1)$$

where  $x$  and  $y$  correspond to activities of excitatory and inhibitory neurons, respectively. We assume The synaptic characteristics  $S(z)$  are given by:

$$S(z) = \frac{1}{1 + e^{-z}}. \quad (2)$$

For Eq. (1), the exactly same equation is assumed in [15]. Also [8] supposes the same equation if  $x$  and  $y$  are swapped each other. We fix parameters as:  $a = b = c = 10.0$ , and  $d = -2.0$  which are often assumed in many publications [1, 2, 17, 18]. We discuss bifurcation structure in  $\rho_x, \rho_y, B$ , and  $\omega$  parameter space. In [8], the bifurcation diagram is obtained in  $\rho_x$ - $\rho_y$  plane. Interaction between a periodic activity in the autonomous system and a periodic forcing may cause a torus (quasi-periodic solution), and various periodic solutions as the frequency entrainment phenomena.

### 3. Method

To investigate stability of periodic solutions appeared in Eq. (1), we use the Poincaré mapping method. Rewrite Eq. (1) as

$$\frac{d\mathbf{x}}{dt} = \mathbf{f}(t, \mathbf{x}, \lambda), \quad \mathbf{x}(0) = \mathbf{x}_0,$$

where  $\mathbf{x} = (x, y)^\top$ ,  $\mathbf{x}_0$  is the initial value, and  $\lambda$  is a parameter.  $\mathbf{f}$  is  $C^\infty$ -class and has the periodicity:  $\mathbf{f}(t) = \mathbf{f}(t + 2\pi)$ . Assuming that a solution function depends on time, the initial value, and the parameter value,

$$\mathbf{x}(t) = \varphi(t, \mathbf{x}_0, \lambda),$$

and we have,

$$\mathbf{x}(0) = \varphi(0, \mathbf{x}_0, \lambda) = \mathbf{x}_0.$$

If a periodic solution is observed, then we recognize  $\mathbf{x}_0$  as a fixed point of the Poincaré mapping applied for every  $t = 2\pi$ :

$$\begin{aligned} T : \mathbf{R}^2 &\rightarrow \mathbf{R}^2 \\ (\mathbf{x}_0, \lambda) &\mapsto \mathbf{x}_1 = T(\mathbf{x}_0, \lambda) = \varphi(2\pi, \mathbf{x}_0, \lambda). \end{aligned} \quad (3)$$

Similarly,  $m$ -periodic point is defined by applying mapping for each  $t = 2\pi m$ , where  $m = 2, 3, \dots$ . The characteristic equation for the fixed point is as:

$$\det \left( \frac{\partial \varphi}{\partial \mathbf{x}_0}(2\pi m, \mathbf{x}_0) - \mu \mathbf{I} \right) = 0, \quad (4)$$

where,  $\partial \varphi / \partial \mathbf{x}_0$ ,  $\mu$ , and  $\mathbf{I}$  are the fundamental matrix of the first variational equation, a multiplier, and a  $2 \times 2$  identity matrix, respectively.

#### 3.1 Brute-force method

To visualize bifurcation structures, we divide a parameter range into small meshes and solve Eq. (1) by an ODE solver for each mesh. Following to the condition Eq. (3), we check the convergence by  $\|T^k(\mathbf{x}_0, \lambda) - \mathbf{x}_0\| < \epsilon$ , where  $k$  is a positive integer. We take  $\epsilon = 10^{-10}$  through this paper. We give an initial value for each computation with the final location  $\mathbf{x}_0$  of the previous mesh. Thus, the result is affected by the direction of the scan direction, but a certain continuity remains in the bifurcation structure. The period is determined by the algorithm presented in [19]; herein, we fix the default initial value as (0.4, 0.3).

We assign colors for  $m$ -periodic solutions as follows: Blue: 1, Red: 2, Magenta: 3, Green: 4, Cyan: 5, Yellow: 6, White: 7, and so on. The black region may include higher periodic solutions, tori, and chaos. Although the brute-force method is a simple strategy and one can comprehend the entire bifurcation structures visually, however, there are several drawbacks; it takes significant time for computation and can follow only one attractor depending on a single initial value, i.e., even if there coexist multiple periodic solutions in the fixed parameter value. Thus, a mesh must be painted using a single color and unstable periodic solutions cannot be visualized.

#### 3.2 Shooting method

By substituting a specific multiplier regarding a local bifurcation into  $\mu$ , we can solve the boundary value problem Eqs. (3) and (4) simultaneously for  $\mathbf{x}_0$  and  $\lambda$  with Newton's method [4].

In this shooting method, accurate calculations are expected that are supported by a quadratic convergence of Newton's method. We assume the tolerant error  $10^{-12}$  for the convergence. All elements of the Jacobian matrix for Newton's method are provided by the fundamental matrix given by solving the first and second variational equations. The mathematical descriptions and methodology are surveyed in [20]. The obtained bifurcation sets may depict a concrete bifurcation structure regardless of the stability for the target periodic solutions. Multi-stable situations can be explained by the bifurcation diagram.

By superimposing both the brute-force and Newton methods, a bifurcation diagram as the topological classification may show the dynamical properties of the system eloquently.

## 4. Results and Discussion

### 4.1 Bifurcations in the $\rho_x$ - $\rho_y$ plane

We fix  $\omega = 1.0$ . The periodic force in Eq. (1) can be regarded as a parameter perturbation in the threshold space  $\rho_x$ - $\rho_y$  [2, 4]. Thus, it is important to investigate bifurcations in this parameter space. Figure 2(a) shows a bifurcation diagram of periodic solutions with  $B = 1.0$ . The symmetrical structure is confirmed and no more periodic islands are found in the larger diagram. If we put  $B = 0$ , at the center  $(\rho_x, \rho_y) = (0, -6)$  [2, 21], the autonomous system has a completely unstable equilibrium point  $(x_0, y_0) = (1/2, 1/2)$  and a stable limit cycle.

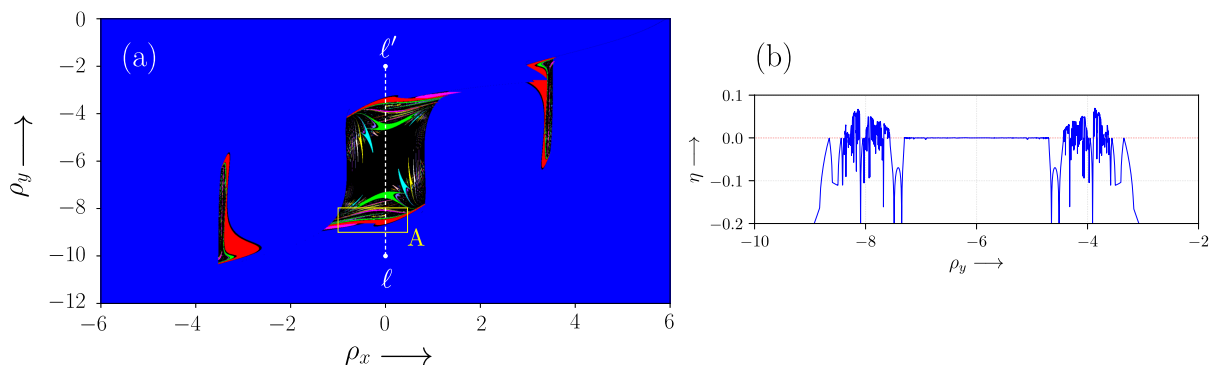


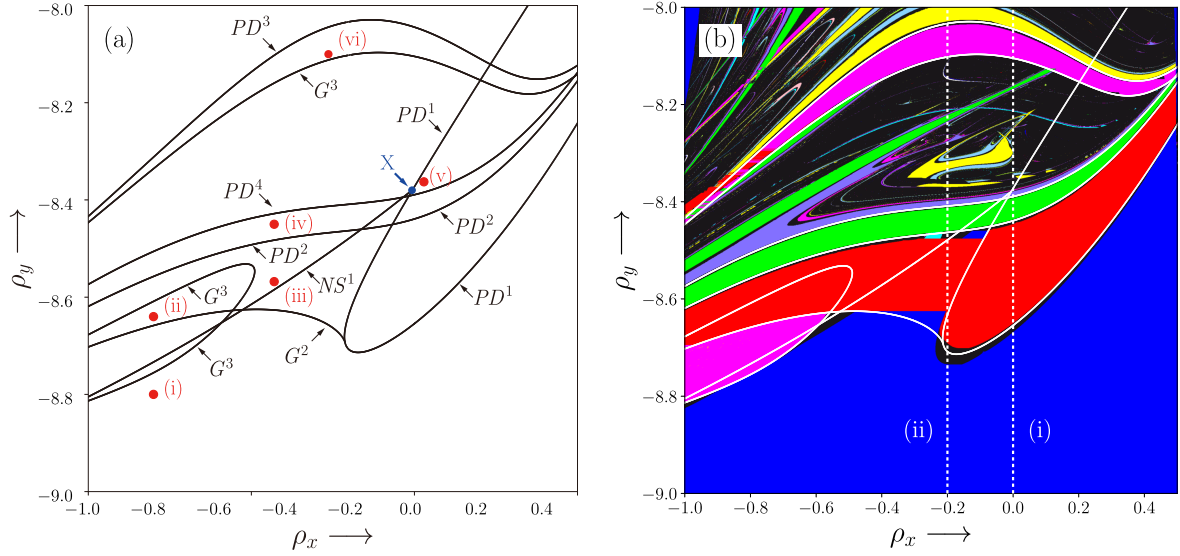
**Fig. 2.** Global bifurcation sets of Eq. (1) in the  $\rho_x$ - $\rho_y$  plane with  $B = 1.0$ , (b): The maximum Lyapunov exponent along  $\ell$ - $\ell'$  (white dashed line) in (a).

Thus, for a parameter set  $(\rho_x, \rho_y)$ , the same topology is given in  $(-\rho_{k1}, -\rho_{k2} - (c - d))$ . This property is based on the symmetry of the sigmoid function which has been investigated thoroughly in [10]. Note that these symmetrical properties depend on the choice of parameters in Eq. (1).

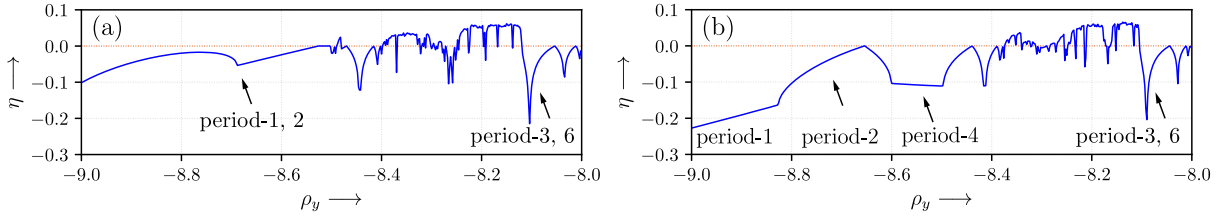
When a periodic external force is applied, because of competition between two periodic cycles, frequency entrainment occurs. That is, many islands surrounded by tangent bifurcation sets appear in Fig. 2(a) and many fish hook structures [22] are found.

Figure 2(b) shows the maximum Lyapunov exponent  $\eta$  along the white dashed line in Fig. 2(a). There is a zero plateau according to a torus response and  $\eta$  is symmetric about  $\rho_y = -6$  according to the above discussed symmetrical properties. The torus response is caused by the mixture of two frequencies based on a limit cycle of the autonomous system and an external force.

Figure 3(a) shows bifurcation sets within the area A in Fig. 2(a) by applying the shooting method. In this figure,  $PD^m$ ,  $G^m$ ,  $NS^m$  are tangent, period-doubling, and Neimark-Sacker (NS) bifurcations for  $m$ -periodic solutions, respectively. Typically, chaotic solutions are given via a period-doubling cascade. The NS bifurcation set is almost hidden by periodic islands. Figure 5 depicts various periodic solutions confirmed on the colored islands (a)-(f) in Fig. 3(a). For each portrait, the parameter values are specified at the top. A red point shows the Poincaré mapping. Figure 3(b) is a superimposed diagram of Fig. 3(a) and the brute-force analysis result. Bifurcation curves obtained by the shooting do not always agree with the colored islands in the brute-force diagram. These mismatched portions are caused by the existence of multi-stable periodic solutions, a long transient response, or bifurcations of unstable periodic solutions as stated in Sec. 3.1. Since the transient responses tend to be long for



**Fig. 3.** (a): Bifurcation sets of Eq. (1) in  $\rho_x$ - $\rho_y$  plane with  $B = 1.0$ , (b): Bifurcation sets on the brute-force computation results.



**Fig. 4.** The maximum Lyapunov exponent along dashed lines in Fig. 3(b). (a):  $\rho_x = -0.2$ , (b):  $\rho_x = 0$ .

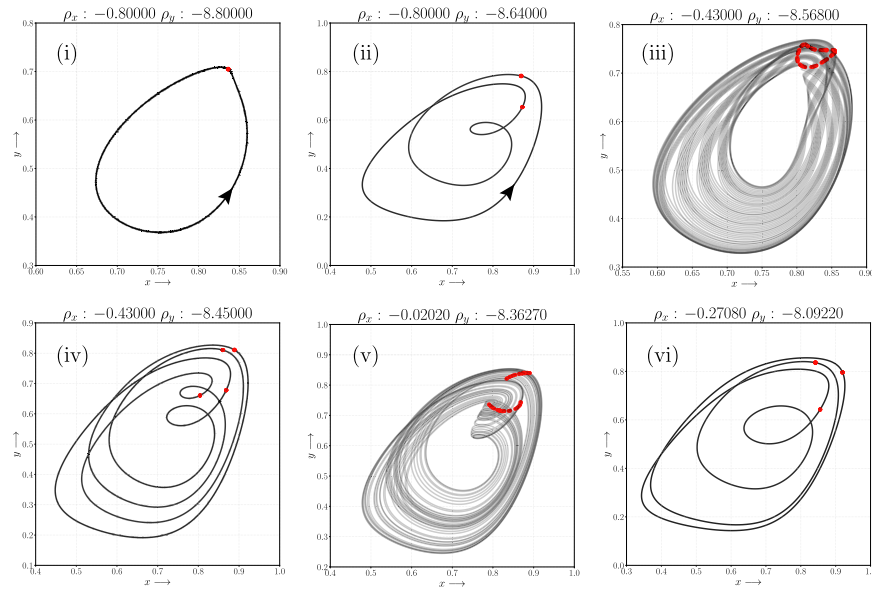


**Fig. 5.** The phase portraits observed in Fig. 3(a). (i): period-1, (ii): period-2, (iii): torus, (iv) period-4, (v): chaos, (vi): period-3.

Eq. (1) when period-doubling or NS bifurcation occurs, black valleys appear between periodic islands. Then bifurcation curves obtained by Newton's method may run through these valleys.

In Fig. 3(a), X shows a codimension-two point connecting  $PD^1$  and  $NS^1$  curves. The  $PD^1$  curve composes an island. For the parameter variation from the blue area to the red area in Fig. 3(b), a stable 2-periodic solution is given inside the red area. There is a period-doubling cascade for this red area, beyond  $PD^2$  and  $PD^4$  curves, we have chaotic attractors; see Fig. 5(v). The cascade structure

hangs out from the  $PD^1$  island edged by the  $G^2$  curve. The upper portion of the period-doubling curve against X flips the stability, i.e., a repeller changes to a 2-periodic repeller inside of  $PD^1$  island, but no further period-doubling is found around X.

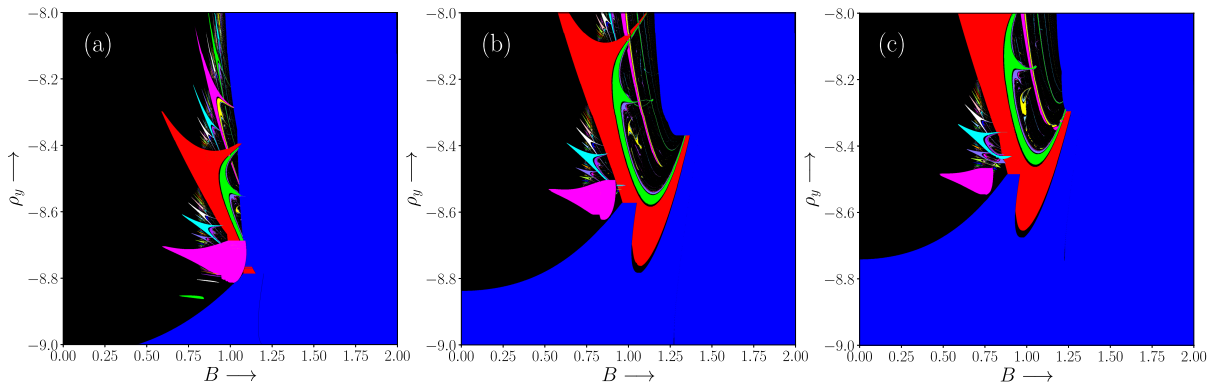
The NS bifurcation curve extends to the left lower part from X; however, the curve is almost hidden by other periodic islands surrounded by  $PD^4$ ,  $PD^2$ , and  $G^3$ . In other words, the brute-force analysis could not detect this curve. According to this NS bifurcation, a period-1 solution changes to a torus; see Fig. 5(iii). Thus there are multi-stable attractors in just the upper portion over this NS curve.

Figure 4 shows the maximum Lyapunov exponent  $\eta$  along the dashed line in Fig. 3(b) with  $\rho_x = -0.3$ . The positive values for  $\eta$  around  $\rho_y = -8.4$  suggest existence of chaotic attractors. In this scan line, there is no chance to have torus response. A smaller absolute value for  $\rho_y$  is needed to obtain a torus response. The  $\rho_x$ - $\rho_y$  diagram Fig. 3(b) shows very different bifurcations structures compared to Noonburg [8] results since a very restricted assumptions are applied in their analysis.

## 4.2 Bifurcations in the $B$ - $\rho_y$ plane

Now, we consider affection of the amplitude  $B$  for the periodic force. Figure 6 shows brute-force bifurcation diagrams in the  $B$ - $\rho_y$  plane with several values of  $\rho_x$ . For each picture, with a small amplitude of the forcing term, there is a torus or a period-1 solution basically, but around  $0.75 < B < 1.25$ , it shows a rich variety of bifurcation sets. This exhibits a validity that we choose  $B = 1$  in Sec. 4.1. Since all pictures keep certain structures, we choose  $\rho_x = -1.0$  here.

Figure 7(a) shows bifurcation sets of periodic solutions. There is a similar structure of the period-doubling island surrounded by  $PD^1$  and a codimension-two point for  $NS^1$  and  $PD^1$  compared with



**Fig. 6.** Brute-force bifurcation diagrams in  $B$ - $\rho_y$  plane. (a):  $\rho_x = -1$ , (b):  $\rho_x = -0.3$ , (c):  $\rho_x = 0$ . Almost identical bifurcation structures are preserved regardless the values of  $\rho_x$ .

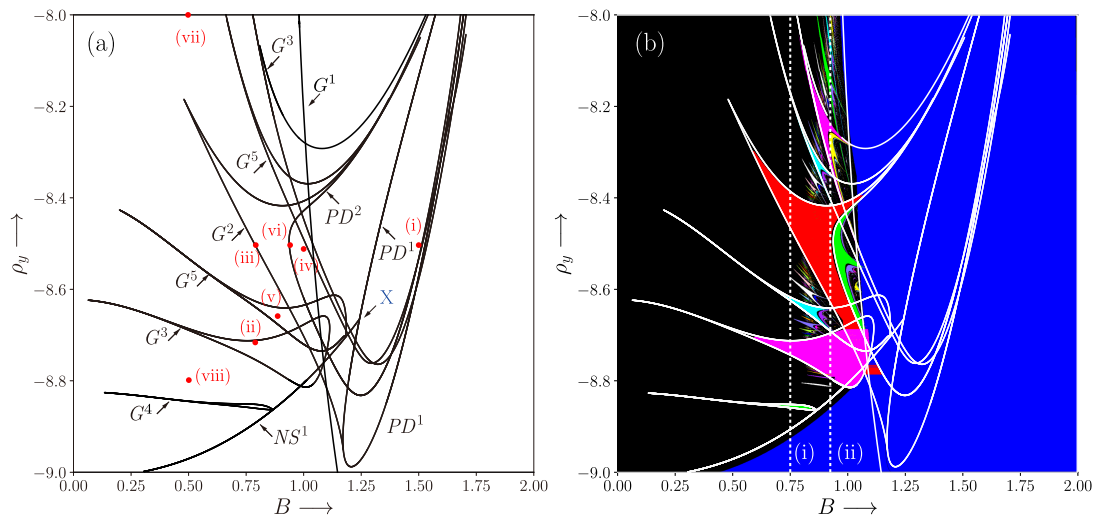


**Fig. 7.** (a): Bifurcation diagram for Eq. (1) in the  $B$ - $\rho_y$  plane with  $\rho_x = -1.0$ . (b): Bifurcation sets with the brute-force computation results.

Fig. 3(a). Many Arnold tongues that show an enormous number of periodic-entrainment areas are confirmed. Figure 7(b) is a superimposed diagram of Fig. 7(a) and the brute-force computations. The period-1 region (Blue) edged by  $G^1$  occupies a wide area and it hides many bifurcation sets in the right half plane.

The period-doubling cascade also hangs out from the  $PD^1$  island. Unlike Fig. 3(b), the black area within  $0 < B < 0.5$  is composed almost entirely of torus responses. Although the autonomous system  $B = 0$  has a limit cycle,  $B > 0$  gives asynchronous behavior. The tips of all tongues seem to be connect to  $B = 0$  axis despite being invisible in this figure. On the  $PD^1$  curve which is completely concealed by the period-1 area, there also exists a point X at which the NS bifurcation curve connects. The NS curve approaches to the lower-left corner, and it connects to the entrainment areas edged by  $G^5$ ,  $G^3$ , and  $G^4$  at every single point that follows specific complex arguments [23]. These connections are not confirmed in Figs. 3(a) and (b).

Figure 8 shows the maximum Lyapunov exponent along scan lines (a) and (b) in Fig. 7(b). For  $B = 0.75$ , almost all  $\rho_y$  give a torus response since  $\eta \approx 0$  except for several periodic entrainment areas. Zero exponents and positive values are found for  $B = 0.9$ , i.e., some chaotic responses are confirmed via the torus breakdown. Therefore, a critical curve that divides the torus and chaotic responses is presumed between these two parameter values. Figure 9 shows the typical attractors given in Fig. 7(b).

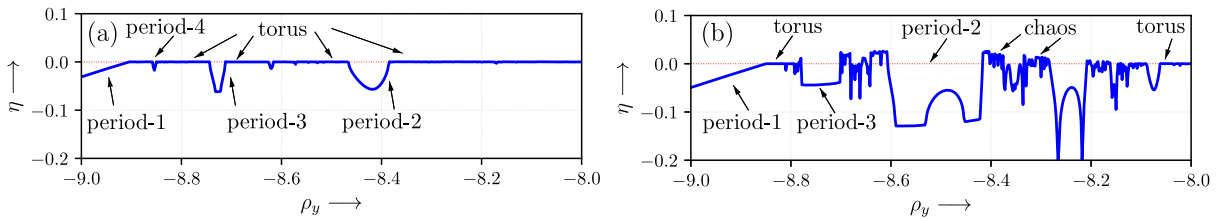


**Fig. 8.** The maximum Lyapunov exponent along the dashed lines (i) and (ii) in Fig. 6(b) with  $\rho_x = -1.0$ . (a):  $B = 0.75$ , (b):  $B = 0.9$ .

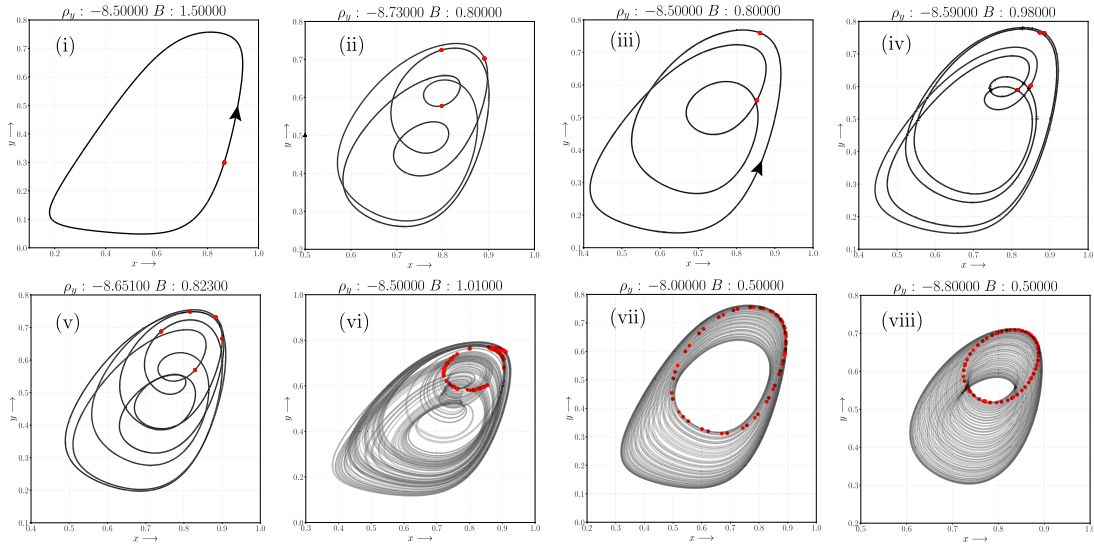


**Fig. 9.** Phase portraits observed in Fig. 7(a). (i): period-1, (ii): period-3, (iii): period-2, (iv): period-4, (v): period-5, (vi): chaos, (vii) and (viii): torus.

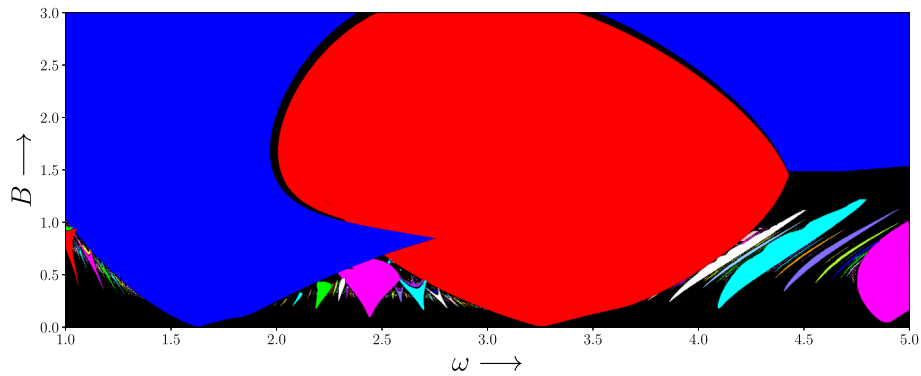
The bifurcation structure of the Duffing–Rayleigh equation [20] closely resembles Fig. 7. For the correspondence between two structures, the angular velocity of a forced term of the Duffing–Rayleigh equation should follow  $\rho_y$  in this paper. In addition, the relative locations of  $NS^1$  and  $G^1$  should be swapped. Regardless of there being no physical relationship between the angular velocity and the threshold value, investigating the correspondence is an interesting topic for the future.

### 4.3 Bifurcations in the $\omega$ - $B$ plane

Bursting responses are frequently observed in neuronal dynamical systems; these are considered to be deeply related to communication between neurons. Periodic bursting may alternate between taking a quiescent state and a spiking state. We have treated bursting responses of several neuronal dynamical systems as bifurcation problems and found a typical structure generating a periodic bursting response. We also expect these responses in Eq. (1) when changing the angular velocity  $\omega$ .

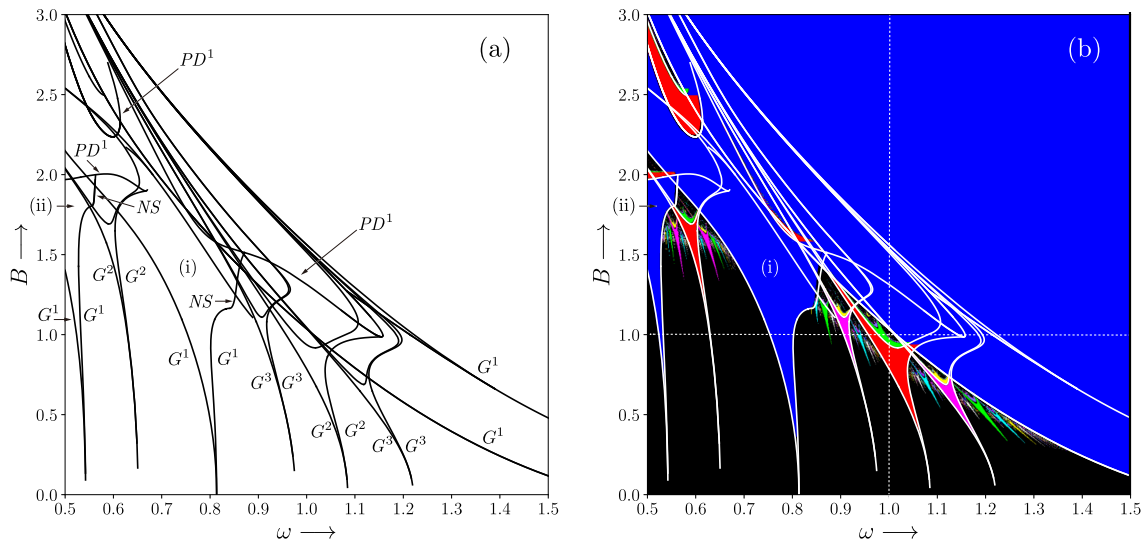
Noonburg [8] investigated some bursting responses in a small range of  $\omega$ . By conflicting between two frequencies (a limit cycle of the autonomous system and a forcing term), the appearance of periodic or quasi-periodic solutions is assumed. A very rough bifurcation diagram in the  $\rho_x$ - $b$  plane is shown analytically but dependency on  $\omega$  is not given.

Figure 10 shows a large brute-force bifurcation diagram in the  $\omega$ - $B$  plane. There exist a huge period-1 and a period-2 entrainment areas in the right portion are found. Reference [15] shows almost the same bifurcation diagram and mainly studies the phase-lock regions surrounded by tangent bifurcations within  $1.5 < \omega < 5.0$ ; however, bursting responses are not discussed, indeed, they do not appear within this parameter range. Note that the direction of the horizontal axis in [15] is flipped to Fig. 10. Hereafter, let us investigate bifurcation structures with smaller  $\omega$  to find bursting responses.

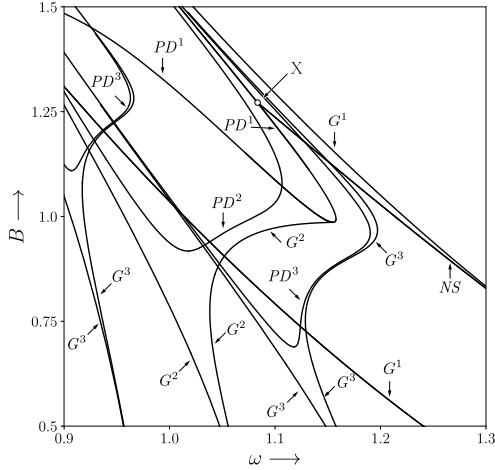


**Fig. 10.** Brute-force bifurcation diagram in the  $\omega$ - $B$  plane in the large.  $\rho_x = -1$ ,  $\rho_y = -8.5$ .

Figure 11 shows the bifurcation diagrams in the  $\omega$ - $B$  plane, where  $0.5 < \omega < 1.5$ . There is a large period-1 area (upper right) is edged by  ${}^1G^1$  that conceals many bifurcation curves. Arnold tongues as frequency entrainment areas according to the standard circlemap are confirmed between two period-1



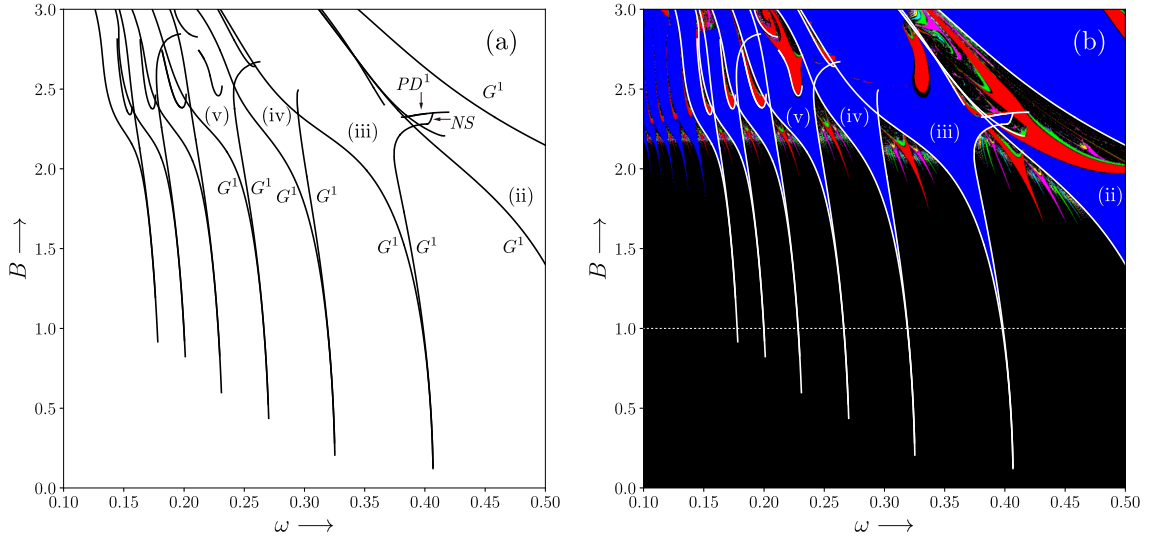
**Fig. 11.** Bifurcation diagrams in the  $\omega$ - $B$  plane,  $0.5 < \omega < 1.5$  with  $\rho_x = -1$ ,  $\rho_y = -8.5$ . (a): Bifurcation sets solved by the shooting method. (b): Bifurcation sets on the brute-force computation result. The horizontal and vertical dashed lines relate to Figs. 3 and 7, respectively.



**Fig. 12.** Enlarged diagram for Fig. 11. A structure which  $PD^1$  and  $NS$  are connected at  $X$  is also confirmed in Figs. 3 and 7.

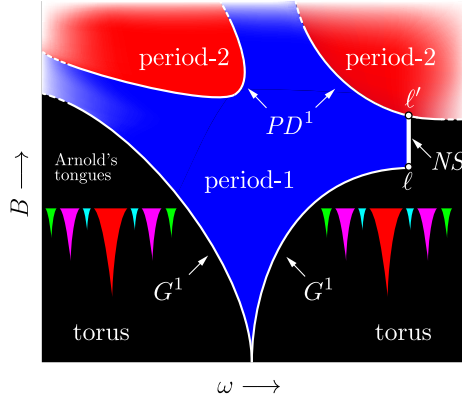
islands labeled (i) and (ii). The black area under these tongues shows torus responses. Figure 12 is an enlargement of Fig. 11; it shows that a period-2 island connects to  $G^2$  and  $NS$  curves like Fig. 3. Almost identical structures are also present in the upper-left corner of Fig. 11.

Figure 13 depicts bifurcations with smaller values of  $\omega$ , i.e., the system is driven by a slower perturbation. There are many similar-shaped period-1 islands, some of which are labeled (ii)–(v). Between two islands, Arnold tongues are lined up. For a smaller value of  $\omega$ , a fractal structure is composed.



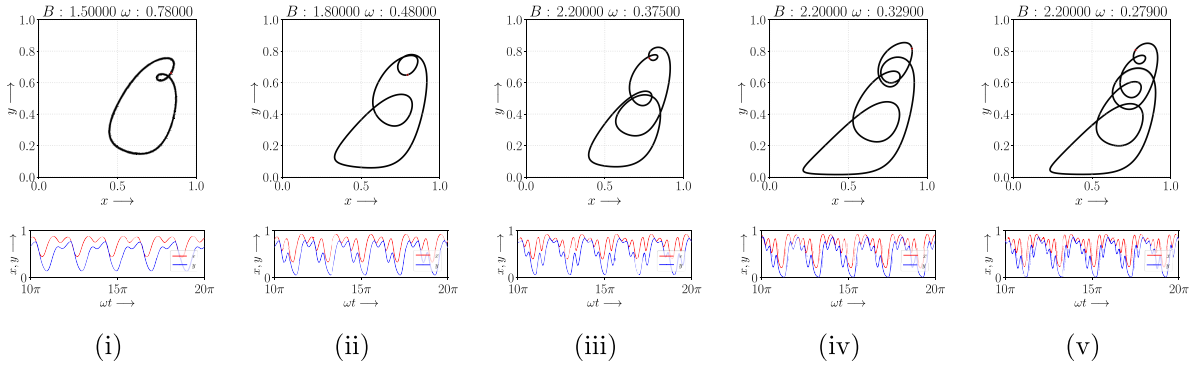
**Fig. 13.** Bifurcation diagrams in the  $\omega$ – $B$  plane,  $0.1 < \omega < 0.5$  with  $\rho_x = -1$ ,  $\rho_y = -8.5$ . (a): Bifurcation sets solved by the shooting method. (b): Bifurcation sets on the brute-force computation result. A dashed line corresponds to the parameter set assumed in Fig. 3.

Figure 14 shows a schematic illustration of a typical period-1 island is shown in The lower period-1 island is edged by the tangent bifurcation curves. Outside of this, Arnold tongues are aligned. A torus response appears under the tongues, and chaotic responses emerge over the tongue. Meanwhile, the right tangent bifurcation curve of the island terminated at  $\ell$ , and the  $NS$  bifurcation curve begins and terminates at  $\ell'$  on another period-doubling bifurcation curve. In the upper portion of the period-1 island, there are two different period-doubling bifurcations. Although a conventional fish-hook structure has a period-doubling bifurcation, this island has multiple period-doubling curves inside. In this situation, a waveform shows a bursting response. The forcing term creates a fundamental frequency and a limit cycle of the autonomous system gives a spiking activity.



**Fig. 14.** Schematic bifurcation structure of a period-1 solution found in Fig. 13. An NS bifurcation bridges a tangent bifurcation at  $\ell$  and a period-doubling bifurcation at  $\ell'$ . The argument of complex conjugate multipliers varies from 0 to  $\pi$  on a unit circle along  $\ell-\ell'$ .

Figure 15 shows various phase portraits and waveforms of periodic bursting responses corresponding to period-1 areas labeled (i)–(v) in Figs. 12 and 13. The bursting pattern within a period-1 area is invariant. Therefore, bifurcation structure analysis reveals the emergence of bursting responses. Chaotic attractors are obtained outside of these period-1 areas; see Fig. 16.



**Fig. 15.** Phase portraits and waveforms of periodic orbits corresponding to period-1 areas labeled (i)–(v) in Figs. 12 and 13. The waveform is retained inside of the island.

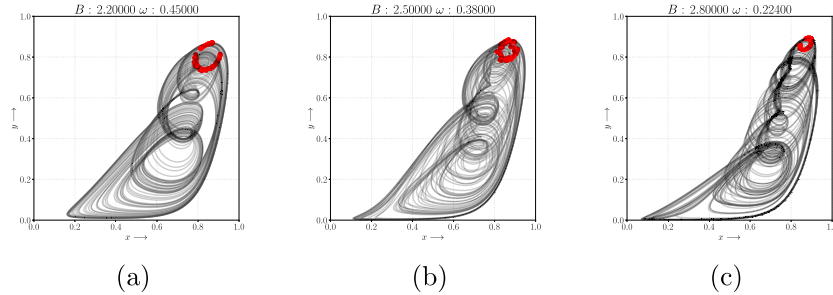


**Fig. 16.** Chaotic attractors bifurcated from bursting responses. (a):  $\omega = 0.45$ ,  $B = 2.2$ , (b):  $\omega = 0.38$ ,  $B = 2.5$ , (c):  $\omega = 0.224$ ,  $B = 2.8$ .

## 5. Conclusions

We investigated the forced WC neuron pairs utilizing both the shooting method and the brute force method in various parameter spaces including threshold values, the amplitude and the angular velocity of the external force. By performing both methods, the topological classification of the periodic solutions is clarified by these diagrams and the maximum Lyapunov exponent. Compared to Noonburg's work, a completely different bifurcation diagram is obtained since they assume a comparatively small

amplitude of the forcing term. However, our analysis suggests that a rich variety of local bifurcations are rather found with a large amplitude of the periodic force.

This paper also suggests the importance of the shooting method, i.e., many bifurcation sets may be hidden when only brute-force analysis is performed. Combining both brute-force and shooting methods can express the topological classification for the given system.

## Acknowledgments

---

TU expresses thanks to Dr. Shigeki Tsuji for his valuable comments. This work is supported partially by KAKENHI grant number 21K04109 and JST Moonshot R&D grant number JPMJMS2021.

## References

---

- [1] E.M. Izhikevich, *Dynamical Systems in Neuroscience: The Geometry of Excitability and Bursting*, MIT Press, 2010.
- [2] F.C. Hoppensteadt and E.M. Izhikevich, *Weakly Connected Neural Networks*, Springer, New York, 1997
- [3] S. Tsuji, T. Ueta, H. Kawakami, and K. Aihara, “An advanced design method of bursting in FitzHugh-Nagumo model,” *Proc. ISCAS 2002*, vol. 1, pp. 389–392, 2002. DOI: 10.1109/ISCAS.2002.1009859
- [4] S. Tsuji, T. Ueta, H. Kawakami, and K. Aihara, “Bifurcation of burst response in an Amari-Hopfield neuron pair with a periodic external force,” *Electrical Engineering in Japan*, vol. 146, no. 2, pp. 43–53, 2004. DOI: 10.1002/eej.10217
- [5] H.R. Wilson and J.D. Cowan, “Excitatory and Inhibitory Interactions in Localized Populations of Model Neurons,” *Biophys. J.*, vol. 12, no. 1, pp. 1–24, 1972. DOI: 10.1016/S0006-3495(72)86068-5
- [6] M.V. Tsodyks, W.E. Skaggs, T.J. Sejnowski, and B.L. McNaughton, “Paradoxical effects of external modulation of inhibitory interneurons,” *J. Neuroscience*, vol. 17, no. 11, pp. 4382–4388, 1997.
- [7] G.B. Ermentrout and D.H. Terman, *Mathematical Foundations of Neuroscience*, Interdiscip. Appl. Math. 35, Springer-Verlag, New York, 2010. <http://dx.doi.org/10.1007/978-0-387-87708-2>
- [8] V.W. Noonburg, D. Benardete, and B. Pollina, “A periodically forced Wilson–Cowan system,” *SIAM Journal on Applied Mathematics*, vol. 63, no. 5, pp. 1585–1603, 2003. DOI: 10.1137/S003613990240814X
- [9] D.J. Pinto, J.C. Brumberg, D.J. Simons, and G.B. Ermentrout, “A quantitative population model of whisker barrels: Re-examining the Wilson–Cowan equations,” *J. Comput. Neurosci.*, no. 3, pp. 247–264, 1996. DOI: 10.1007/BF00161134
- [10] R. Decker and V.W. Noonburg, “A periodically forced Wilson–Cowan system with multiple attractors,” *SIAM Journal on Mathematical Analysis*, vol. 44, no. 2, pp. 887–905, 2012. DOI: 10.1137/110823365
- [11] E. Ledoux and N. Brunel, “Dynamics of networks of excitatory and inhibitory neurons in response to time-dependent inputs,” *Frontiers in Computational Neuroscience*, vol. 5, no. 25, pp. 1–17, 2011. DOI: 10.3389/fncom.2011.00025
- [12] T. Ueta, G. Chen, T. Yoshinaga, and H. Kawakami, “A numerical algorithm for computing Neimark–Sacker bifurcation parameters,” *Proc. ISCAS 1999*, vol. 5, pp. 503–506, 1999. DOI: 10.1109/ISCAS.1999.777619
- [13] T. Ueta, S. Tsuji, T. Yoshinaga, and H. Kawakami, “Calculation of the isocline for the fixed point with a specified argument of complex multipliers,” *Proc. ISCAS 2001*, vol. 2, pp. 755–758, 2001. DOI: 10.1109/ISCAS.2001.921442
- [14] T. Ueta and G. Chen, “On synchronization and control of coupled Wilson-Cowan neural oscillators,” *Int. J. Bifurc. Chaos*, vol. 13, no. 01, pp. 163–175, January 2003. DOI: 10.1142/S0218127403006406

- [15] A. Pérez-Cervera, T.M. Seara, and G. Huguet, “Phase-locked states in oscillating neural networks and their role in neural communication,” *Commun. Nonlinear Sci. Numer. Simulat.*, vol. 80, 104992, 2020. DOI:10.1016/j.cnsns.2019.104992
- [16] M. Benayoun, J.D. Cowan, W. van Drongelen, and E. Wallace, “Avalanches in a stochastic model of spiking neurons,” *PLoS Computational Biology*, vol. 6, no. 7, e1000846, 2010. DOI: 10.1371/journal.pcbi.1000846
- [17] R.M. Borisyuk and A.B. Kirillov, “Bifurcation analysis of a neural network model,” *Biological Cybernetics*, vol. 66, pp. 319–325, 1992. DOI: 10.1007/BF00203668
- [18] E.M. Izhikevich, “Neural excitability, spiking and bursting,” *Int. J. Bifurc. and Chaos*, vol. 10, no. 06, pp. 1171–1266, 2000. DOI: 10.1142/S0218127400000840
- [19] T. Gray and J. Glynn, *Exploring Mathematics with Mathematica*, Chapter Seven, Addison-Wesley, 1991.
- [20] K. Tsumoto, T. Ueta, T. Yoshinaga, and H. Kawakami, “Bifurcation analyses of nonlinear dynamical systems: from theory to numerical computations,” *NOLTA*, vol. 3, no. 4, pp. 458–476, 2012. DOI: 10.1588/nolta.3.458
- [21] P.C. Bressloff, “Metastable states and quasicycles in a stochastic Wilson–Cowan model of neuronal population dynamics,” *Pys. Rev. E.*, no. 82, 051903, 2010. DOI: 10.1103/PhysRevE.82.051903
- [22] T. Matsumoto, L.O. Chua, and M. Komuro, “The double scroll,” *IEEE Trans. Circuits Syst., CAS-32*, no. 8, pp. 797–818, 1985.
- [23] T. Ueta, S. Tsuji, T. Yoshinaga, and H. Kawakami, “Calculation of the isocline for the fixed point with a specified argument of complex multipliers,” *Proc. ISCAS2001*, vol. III, pp. 281–284, Sydney, May 2001. DOI: 10.1109/ISCAS.2001.921442